ELSEVIER

International Journal of Heat and Fluid Flow 21 (2000) 1–10

International Journal of HEAT AND FLUID FLOW

www.elsevier.com/locate/ijhff

Development of a turbulent jet generated by a mixer in weak co-flow and counter-flow

Per Petersson, Magnus Larson *, Lennart Jönsson

Department of Water Resources Engineering, University of Lund, P.O. Box 118, S-22100 Lund, Sweden

Received 28 April 1998; accepted 10 October 1999

Abstract

Laser doppler velocity measurements of the axial, tangential, and radial velocity components were performed in a turbulent jet generated by an impeller operating in a weak co-flow and counter-flow. The measurements were carried out downstream of a model impeller placed in a glass-walled flume, which was either closed-off or operated with a small base flow. For the closed-off flume case a return flow was produced causing the jet to develop in a weak counter-flow, whereas in the base flow case the jet evolved in a weak co-flow. The jet development in these two types of flow, essentially representing perturbations of the classical problem of a jet in an unconfined, quiescent ambient fluid, was compared with respect to mean velocities and integral flow properties such as jet spread, volume flux, and momentum flux.

Keywords: Mixer; Jet; Turbulence; Shear flows; Impeller; Self-similarity; Laser Doppler Velocimeter

Notation

a	distance from virtual origin to impeller blades
b	jet width based on the radial distance where $=0.5\ U_m$
C_u	non-dimensional coefficient (mean axial velocity distribution)
C_w	non-dimensional coefficient (mean tangential velocity distribution)
D	impeller diameter
G_x	axial flux of linear momentum corrected for pressure (jet thrust)
G_φ	axial flux of angular momentum
K_e	entrainment coefficient
N	impeller speed
R	impeller radius
r	radial coordinate
Q	volume flux
Q_0	volume flux through impeller
S	swirl number
U	axial velocity
$\bar{U}$	mean axial velocity
U_a	mean longitudinal velocity in the ambient fluid
U_{a0}	mean longitudinal velocity in the ambient fluid upstream impeller
U_m	maximum of mean axial velocity
U_p	peripheral velocity of impeller blades
u	rms value of axial velocity unsteadiness
V	radial velocity
$\bar{V}$	mean radial velocity
v	rms value of radial velocity unsteadiness
W	tangential velocity
$\bar{W}$	mean tangential velocity
W_m	maximum of mean tangential velocity
w	rms value of tangential velocity unsteadiness
x	horizontal coordinate
y	lateral coordinate
z	vertical coordinate
ρ	fluid density
ξ	$r/(x+a)$, similar radial coordinate

1. Introduction

In many environmental and technical/industrial applications, there is a need to artificially induce flows in fluids and fluid mixtures. The purpose of such flow generation could be to transport substances, keep solids in suspension, homogenize fluids with different properties, dissolve matter in liquids, enhance biological and chemical reactions, or modify the thermal conditions in a fluid. A submersible mixer is a flexible and efficient device for inducing artificial flows. The mixer consists of an impeller, which is basically a propeller operating at static conditions, and a motor driving the impeller. The rotating impeller generates a swirling jet with an initial size, velocity, and direction depending on the characteristics and orientation of the impeller. The swirling jet penetrates through the fluid and grows in size as it entrains ambient fluid; simultaneously, a large-scale motion is induced in the fluid that largely depends upon the boundary geometry. This large-scale flow pattern is in many applications of decisive importance for achieving the

* Corresponding author. Fax: +46-46-222-4435.
E-mail address: magnus.larson@tvrl.lth.se (M. Larson).

0142-727X/00/$ - see front matter
PII: S0142-727X(99)00075-2

desired effects with the flow generation. Most mixer applications involve complex fluid dynamics regarding both the impeller jet and the induced large-scale motion that must be understood in detail to maximize the efficiency of the mixing operation.

Conventionally, mixers have mainly been used in fluid bodies of relatively small scale, but there is a potential for also using mixers in larger fluid bodies (Jönsson and Rissler, 1991; Stephens and Imberger, 1993). A mixer with a large diameter may be used to generate large-scale circulation, which is needed in environmental applications where significant water masses should be mixed. However, little guidance is available at present to design and operate mixers for a specific application because of the limited knowledge about flows generated by mixers. Comprehensive investigations on the properties of swirling jets generated by impellers are in general lacking. As a result, the design and choice of a mixer for a certain application is largely based on empirical information. Thus, there is a need for fundamental studies on mixer fluid dynamics that elucidate the basic properties of swirling jets, and for validation and development of reliable computational models to describe impeller flows. An important aspect when applying mixers to limited fluid volumes is the effect of the circulation (natural or induced by the jet) on the development of the impeller jet. Even a weak flow in the surrounding fluid may decisively affect the jet properties, at least some distance downstream of the impeller.

Swirling jets appear in many other applications besides mixer-induced flows. Although the characteristics of these jets initially often differ markedly from jets generated by mixers, analogies can be found, especially some distance away from the jet source. Propellers are often employed for the propulsion of airborne and marine vehicles, and the flow in the slipstream or wash has similarities with the swirling jet generated by an impeller. In studies of propeller flows the focus is typically on the velocity field in the vicinity of the propeller, and the development of the downstream flow field is of less concern. In contrast, both the generation and the downstream development of the swirling jet are of primary interest in mixer-induced flows, as well as any interaction with the flow boundaries and secondary flows induced by the jet. The limited number of detailed investigations of the velocity field downstream of an impeller or propeller are derived mainly from the fields of aerodynamics (Biggers and Orloff, 1975; Lepicovsky and Bell, 1984; Lepicovsky, 1988), naval architecture (Min, 1978; Kobayashi, 1981; Hyun and Patel, 1991a,b; Hamill and Johnston, 1993), and turbomachinery (Strazisar and Powell, 1981). Reference to these works are made not only because of possible similarities with the jet behavior in the present study, but also regarding measurement techniques employed to determine the generated velocity field. High-resolution measurements of the velocity field generated by an impeller or propeller are often difficult to perform requiring experience of advanced measurement techniques.

In this study the velocity field downstream of a model impeller operating in water was measured using a two-component Laser Doppler Velocimeter (LDV), both for the case of a weak co-flow and counter-flow. The investigation focussed on the spatial development of the mean velocity in the axial, radial, and circumferential direction, although simultaneous measurements were performed on the velocity unsteadiness from which turbulence characteristics were inferred (not discussed here, see Petersson, 1996). The measurements extended up to 12 impeller diameters downstream of the blades displaying the properties of the generated swirling jet both in the zone of flow establishment (ZFW) (Albertson et al., 1950) and the zone of established flow (ZEF). The division between these zones was made based on similarity of the mean axial velocity profile. Integral properties of the flow such as volume and momentum flux were computed from the measured velocity profiles. The transverse spreading of the impeller jet and its development towards self-similarity (Townsend, 1976) were examined and compared with non-swirling jets (Albertson et al., 1950; Hussein et al., 1994) and swirling jets generated by other means (Rose, 1962; Chigier and Chervinsky, 1967; Pratte and Keffer, 1972).

The motivation for studying the development of impeller jets in weak co-flow and counter-flow was the possible application of mixers in large-scale fluid bodies, where it is expected that the fluid outside the jet would be moving at low velocity. As will be shown in the following, even low ambient velocities perturb the condition at the jet boundary significantly affecting jet properties. Thus, it is of importance to determine how the jet will respond to the circulation in the ambient fluid when designing a mixer operation for large-scale applications. In many cases the circulation is induced by the jet itself through the entrainment of ambient fluid, creating a complex interaction between the jet and the ambient circulation. The present study constitutes a first step towards quantifying how a small perturbation at the boundary of a turbulent jet will affect the jet properties.

2. Laboratory experiments

The swirling jet investigated in these experiments was generated with a 1:10 model of the impeller from a Flygt 4501 mixer (Fahlgren and Tammelin, 1992). The three-blade impeller had an overall diameter of $D = 0.078$ m and a hub diameter of 0.023 m (see Fig. 1(a)). The axial extension of the hub was 0.020 m. With only three blades, blade-to-blade interaction was limited and the blade passages were important for the flow development close to the impeller. During the measurements, the impeller was mounted on a model motor that was operated at a fixed rotational speed N

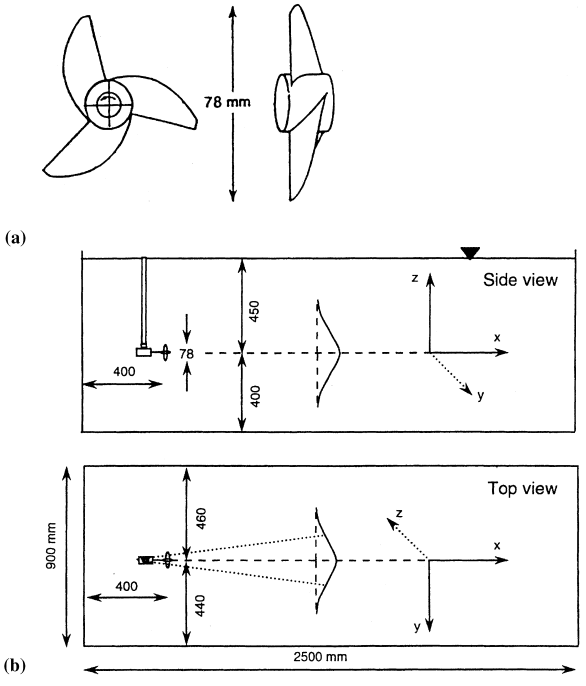

Fig. 1. Schematic description of the experimental-setup, (a) impeller and (b) flume layout and mixer location (closed-flume case shown).

throughout a specific experimental case. Observations indicated that the drift of the motor speed during a run was of the order of 1%.

Measurements of the axial (U), tangential (W), and radial (V) velocity components were carried out downstream of the model impeller. The mixer was placed in a glass-walled flume that was 21 m long with a 0.9×0.9 m^2 cross-sectional area (see Fig. 1(b)). The water depth in the flume was 0.85 m and the impeller was located as centered as possible 0.45 m below the water surface. A two-component Laser Doppler Velocimetry (LDV) system (TSI system 90-3) was used to perform the velocity measurements, making it necessary to make two sets of measurements at each point to obtain all three velocity components. Both the mean velocities ($\bar{U}, \bar{W}$ and $\bar{V}$) and the velocity unsteadiness were recorded (Petersson, 1996; Petersson et al., 1996a,b), although only the former will be discussed here. Most of the measurements were made through straightforward time-averaging using a sampling time short enough to ensure that the velocity fluctuations of interest were resolved. However, limited phase-averaging was also performed to determine the effects of the blade periodicity close to the impeller. To allow for efficient and accurate data collection, a computer-controlled traversing system was developed that automatically moved the LDV probe in two perpendicular directions. In the third direction, the probe was moved by hand along a rigid fixed rail aligned with the wall of the flume.

The measurements in the impeller jet were carried out with a weak co-flow or counter-flow in the ambient water. The co-flow was generated by introducing a small base flow in the flume, whereas the counter-flow was obtained by closing off the flume which induced a recirculation in the ambient. The velocity of the added base flow upstream of the impeller (U_{a0}) was uniform over the flume cross-section (confirmed by measurements) and several different flow velocities were investigated initially ($U_{a0} = 0.05, 0.10, 0.20$ m/s). In all experimental cases discussed here regarding the co-flow, a velocity of 0.05 m/s was employed upstream of the impeller (see Petersson, 1996 for results including other co-flow velocities). This ambient velocity was sufficient to prevent a return flow to develop over the distance of observation. In the counter-flow experiment, the flume was closed-off to form a 2.5 m long section with the impeller located 0.4 m from the back wall. Complete cross-sections of the jet were traversed by the LDV at selected locations downstream of the impeller, from approximately $0.128D$ to $12D$. Downstream of $12D$ the conditions became too complicated to regard the flow as a jet developing in an ambient fluid. Two different impeller speeds were used in the closed-off flume, namely $N = 1200$ and 1800 rpm, whereas only $N = 1800$ rpm was employed in connection with the base flow.

The characteristic length scale for the jet in this experiment was D (or, equivalently, the impeller radius R), whereas the velocity scale could be taken as the peripheral velocity of the impeller (tip speed) $U_p = 2\pi NR$, at least close to the impeller. Thus, the ratio U_{a0}/U_p would characterize the effect of the ambient fluid velocity on the initial jet development in co-flow. For the co-flow cases discussed here, $U_{a0}/U_p = 0.007$ and it is not expected that there would be a great effect from the ambient flow on the initial jet development, which was confirmed by measurements (discussed later). Close to the impeller, the typical maximum value of the mean axial velocity in the jet was about 20–30% of U_p. Further downstream of the impeller, it is expected that the ratio U_a/U_m will instead determine the influence of the ambient flow on the jet development, where U_a is the representative ambient velocity and U_m the mean axial velocity at the jet center line (taken at a specific downstream location). This ratio took on values at least an order of magnitude larger than the corresponding ratio at the impeller (U_{a0} divided by the maximum mean axial velocity), which was enough to significantly influence the jet properties.

The low values of U_{a0}/U_p indicate that the impeller flow had little similarities with most airplane and ship propellers close to the source of generation. However, for the primary application of interest in this study, the values of U_{a0}/U_p selected in the experiments were in agreement with typical prototype values. For example, using mixers for improving the circulation in small water bodies would encompass mixers with impeller diameters of 1–2.5 m operating at 0.5–2.0 Hz. Such prototype conditions produce reference values that well correspond to what was used in the present experiments. The measurement uncertainty of the experiments has been discussed in detail in Petersson (1996) and Petersson et al. (1996a).

3. Results

3.1. Flow structure

The development of the flow immediately downstream of the impeller was very similar for the co-flow and counter-flow cases and may be schematically described as follows. A complicated flow field developed close to the impeller that was a function of the flow generation in distinct areas around the impeller such as the hub, mid-span, and tip areas (Hyun and Patel, 1991a,b). The rotating hub created an inner solid-body rotation with a peak tangential velocity at a position corresponding to the hub radius. Simultaneously, a wake was formed downstream of the hub that was a function of the hub geometry. Away from the hub, mainly in the mid-span region, the flow was periodic due to the blade passage. After the fluid left the blade, a wake was formed that was responsible for the initially very high turbulence intensities found in the impeller jet. The generated blade wakes gave rise to velocity gradients in the circumferential direction which in turn increased the turbulence generation and turbulent mixing. At the blade tips, vortices formed as the boundary layer on the blades rolled up from the pressure side to the suction side of the blade tips resulting locally in negative velocities relative to the mean flow direction. The tip vortices surrounded the jet for some distance downstream. Fluid was not in direct contact with the blades and the hub passed through the impeller disk with little increase in turbulence intensity and flow direction.

As a result of the varying flow characteristics in the circumferential direction, the flow field downstream of the impeller was periodic which affected both the mean velocities and the turbulence. With increasing radial distance from the hub the length between the blades in the circumferential direction increased and blade-to-blade interaction became limited, and the periodic behavior was therefore a more dominant part of the flow. Towards the blade tips, the roll-up of the tip vortices further complicated the flow picture. The gradients in the circumferential direction gradually diminished with distance downstream and the flow became axisymmetric at some point. Spectral analysis together with limited phase-averaged measurements were used in the present study to investigate the occurrence of periodicity in the flow field (see also Petersson, 1996). Up to $1D$ the periodicity was found to be marked after which the diffusion of the turbulence from the blade wakes seemed to proceed quickly, and the periodicity had disappeared after $2D$. The focus here is on the development of the impeller jet flow in the region where the jet is axisymmetric, so the periodicity in the flow due to blade passages will not be discussed further. Hyun and Patel (1991b) made phase-averaged measurements downstream of a propeller and found the flow to be axisymmetric at a distance of about $2D$, although it should be kept in mind that they studied a ship propeller

operating in a considerably larger relative co-flow velocity ($U_{a0}/U_p = 0.26$). In general, the location where the jet becomes axisymmetric depends on the rotational speed of the impeller, the number of blades, and the overall impeller design, as well as the ambient flow conditions.

When the impeller was operating in the closed-off section of the flume, it was affected by the circulation pattern induced in the limited water mass. The impeller generated a swirling jet that increased in size as it developed downstream. Simultaneously, a return flow was created outside the jet supplying the jet with water for the entrainment and the initial jet discharge. The return flow also consumed jet momentum that caused a reduction in the jet velocity compared to a free jet. Fig. 2(a) illustrates the schematic flow structure for the case of the closed-off flume. Close to the impeller the ambient flow conditions had little effect on the jet development; however, farther downstream the conditions in the ambient significantly influenced the jet properties, as will be shown later. Approximately 12D from the impeller the direct effects of the sidewalls became marked, restricting the jet development, and no measurements were made further downstream. Over the distance of measurements the flow was similar to a jet developing in a counter-flow, although the situation was somewhat different from a simple counter-flow (Abramovich, 1963) since the recirculating water fed the jet and the return flow was continuously reduced. Some low-frequency velocity fluctuations appeared in the flow that were attributed to slow oscillations in the jet position resulting from interaction between the recirculating water and the jet (compare Shih and Ho, 1994).

Fig. 2(b) displays the schematic flow structure for the base flow case. Contrary to the closed-flume case, the entrained water had a velocity component in the jet direction and thus contributed with momentum to the jet. Measurements at different locations outside the jet showed that the ambient flow was approximately evenly distributed over the cross-section. The continuous entrainment of ambient water reduced the co-flow velocity gradually. From the original velocity of 0.05 m/s upstream the impeller, the velocity in the ambient flow decreased slowly to about zero at 12D. Downstream of this location recirculation could be observed at the surface, where the water was flowing backwards in a zone extending between approximately 14D–16D. The disturbed water found in this recirculation zone did not influence upstream water, and instead it was observed that the recirculated water was transported downstream with the mean flow. The co-flow stabilized the jet path and the deflection or oscillation of the jet was much reduced in comparison to the closed tank. Low-frequency fluctuations were still present but the magnitude was considerably smaller than in the counter-flow experiment.

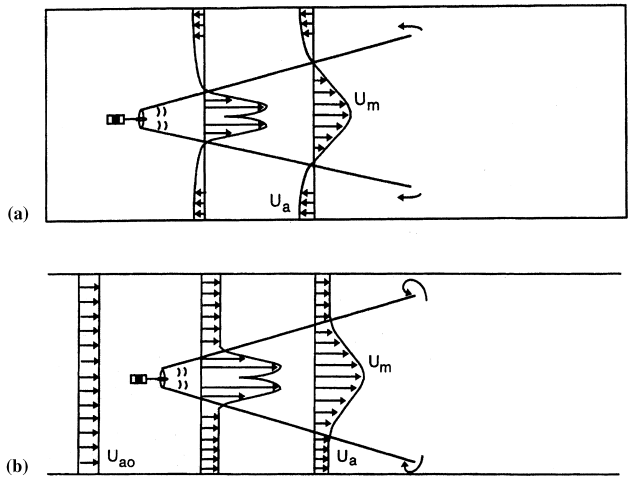

Fig. 2. Flow structure for the case of an impeller operating in (a) a closed-off section of the flume and (b) in an open flume with a base flow (jet size and base flow exaggerated).

3.2. Mean velocities

The principal features of the spatial development of the mean jet velocity components were similar for the closed-off flume and base flow case, although the numerical values of some basic jet properties differed as will be discussed shortly. Fig. 3(a), (b) and (c) show the radial distribution of the mean axial, tangential, and radial velocity, respectively, for the base flow case ($N = 1800$ rpm) at selected downstream locations. Only half of the impeller jet is displayed in the figures; in several cases the entire jet was traversed to confirm that the velocity profile was axisymmetric. The peripheral velocity of

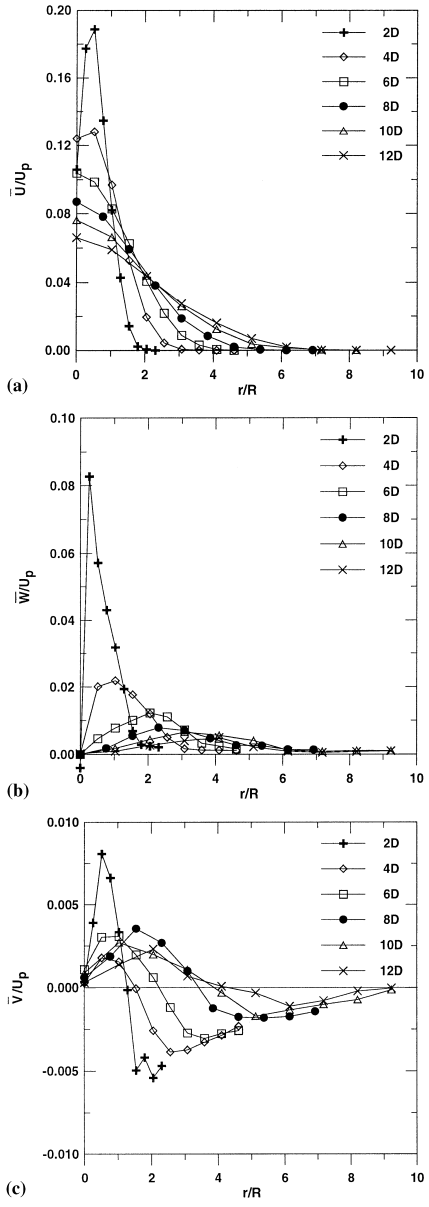

Fig. 3. Mean velocity profiles for the co-flow experiment, (a) axial, (b) tangential, and (c) radial velocities.

the impeller (U_p) was used to normalize the measured velocities in the figures and the radial distance r was normalized with the impeller radius R. The mean velocity of the ambient flow measured at a particular cross section was subtracted from $\bar{U}$ before plotting in Fig. 3 (the ambient velocity was approximately uniform outside the jet region).

Immediately downstream of the impeller a distinct trough is seen in the distribution of $\bar{U}$ that is mainly an effect of the blocking hub (see off-axis peak at $x = 2D$ in Fig. 3(a)). Since the impeller used in the present investigation produced a fairly weak degree of swirl the trough was rapidly "filled" a short distance downstream of the impeller, mainly because of turbulent diffusion. From approximately $4D$ the maximum velocity appears at the jet centerline and the $\bar{U}$-profile starts to attain a Gaussian shape. The mean tangential velocity has a very pronounced peak close to the impeller that is reduced at a high rate in the downstream direction, simultaneously as the position of the peak is displaced out from the jet center (Fig. 3(b)). The high peak near the impeller is associated with a solid-body rotation of the water that becomes less important further away from the impeller where the main portion of the swirl flow has the properties of a free vortex. All measurements of $\bar{W}$ showed values close to zero in the jet center indicating that the alignment of the experimental setup was satisfactory during the experiments.

Fig. 3(c) shows that the radial component $\bar{V}$ is directed out from the jet center at every location from $2D$ to $12D$ (positive velocity represents an outflow from the jet center). Towards the jet edge, the flow direction is reversed and a radial inflow (entrainment) into the jet is clearly seen. In the jet center values close to zero are obtained, which is expected due to symmetry. Very close to the impeller ($x < 2D$) $\bar{V}$ is mainly directed towards the jet center (measurements not shown here, see Petersson et al., 1996a). This inflow is caused by the radial pressure gradient imposed by the swirl and the wake formed behind the hub. Partly due to this inflow the low velocity core is accelerated and disappears rather quickly.

Close to the impeller, the effect of a weak ambient velocity on the jet development is negligible and the impeller characteristics determine the mean velocity profiles. Fig. 4(a) and (b) display measured $\bar{U}$- and $\bar{W}$-profiles for $N = 1800$ in the ZFE, which was defined based on the location where $\bar{U}$ displayed self-similarity in analogy with Albertson et al. (1950) (for a more extensive discussion of how ZFE and ZEF was distinguished in this study, see next section). A distance $0.128D$ downstream of the impeller there is essentially no difference between the co-flow and counter-flow experiments (Fig. 4(a)). As previously mentioned, the hub blockage produced a distinct trough in $\bar{U}$ with an off-axis peak at about $r/R = 0.5$ (location of maximum thrust created by the blades). At $2D$ some differences between the $\bar{U}$-profiles are noticeable, especially near the jet center where the trough is more rapidly "filled" for the counter-flow experiment. The $\bar{W}$-profiles at $0.128D$ display two clear peaks; the inner one is generated by the rotating hub and the outer one by the impeller blades. At $2D$ the two peaks have merged to one, simultaneously as the $\bar{W}$-profiles have become much flatter. The differences between the $\bar{W}$-profiles for co-flow and counter-flow at $0.128D$ are mainly attributed to a lower data rate obtained in the co-flow experiment.

In the ZEF the jet differs markedly for the co-flow and counter-flow experiments, although the overall shape of the $\bar{U}$- and $\bar{W}$-profiles are quite similar in the two experiments (see Fig. 5(a) and (b)). The $\bar{U}$-profiles measured in the co-flow are more narrow and the spread of the jet is considerably less. At $4D$ the $\bar{U}$-profile measured in the counter-flow has attained a Gaussian shape with the maximum (U_m) at the jet center, whereas U_m for the co-flow is still slightly off-axis. Farther downstream a Gaussian shape is a good approximation for the

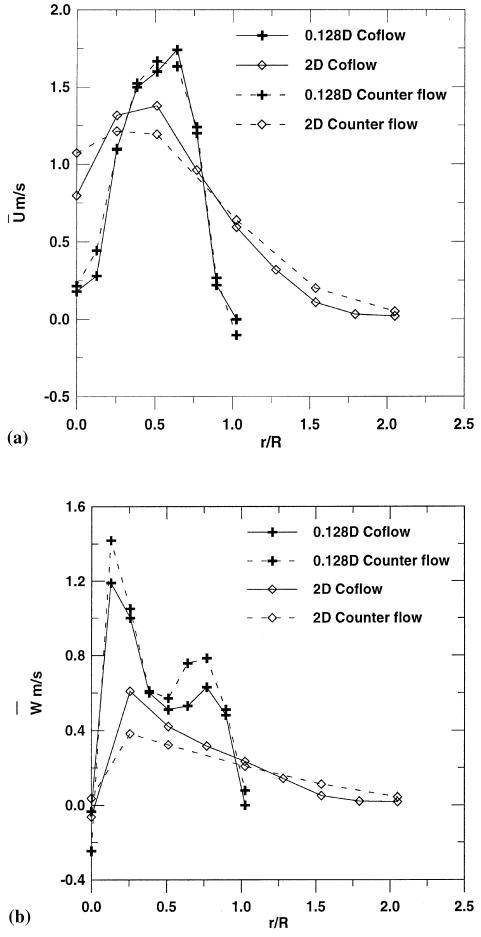

Fig. 4. Comparison between mean velocity profiles for co-flow and counter-flow in ZFE, (a) axial and (b) tangential velocities.

$\bar{U}$-profile, both in the co-flow and counter-flow. The values of $\bar{W}$ are larger in the co-flow experiment, but the maximum in $\bar{W}$ (W_m) is found approximately at the same radial location for the two experiments. Similar to $\bar{U}$ and $\bar{W}, \bar{V}$ displayed profiles that were more narrow for the co-flow compared to the counter-flow experiment.

3.3. Self-similarity

In the vicinity of the impeller the jet is a function of the impeller characteristics such as diameter, rotational speed, number of blades, and blade shape. The periodicity of the blades introduced in the flow has basically disappeared $1D$ downstream of the impeller and the jet may be regarded as completely axisymmetric from $2D$ (Petersson, 1996). Furthermore, after about $4D$ the $\bar{U}$-profiles exhibit self-similar properties, that is, appropriately scaled all $\bar{U}$-profiles can be described by the same function, which is a Gaussian curve. The normalization of $\bar{U}$and r was done with U_m and $x + a$, respectively, where a is the location of a virtual origin for the impeller jet (how this origin was determined is discussed in the next section). A common criterion for distinguishing between ZFE and ZEF is whether $\bar{U}$ displays self-similarity (Albertson et al., 1950); this criterion was also employed in the present study, as indicated in the previous section. Fig. 6 illustrates $\bar{U}/U_m$ as a function of $\xi = r/(x + a)$ for the co-flow and counter-flow experiments, together with least-square fitted Gaussian curves given by

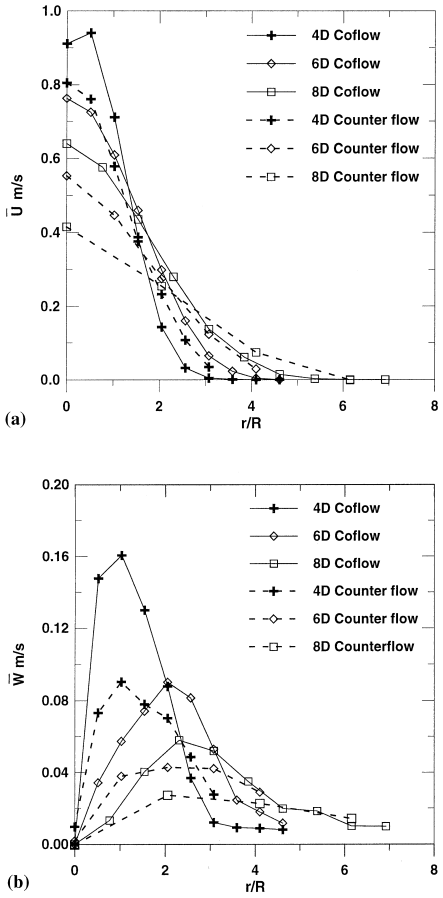

Fig. 5. Comparison between mean velocity profiles for co-flow and counter-flow in ZEF, (a) axial and (b) tangential velocities.

$$\frac{\overline{U}}{U_{\mathrm{m}}} = \mathrm{e}^{-C_u \xi^2}, \tag{1}$$

where C_u is an empirical coefficient. The figure summarizes the measurements of $\bar{U}$ carried out from $4D$ to $12D$, except the $\bar{U}$-profiles measured at $4D$ for the co-flow since it showed a slight off-axis peak (see Fig. 5(a)). The different jet widths are clearly displayed and C_u was determined to 41 and 92 for counter-flow and co-flow, respectively. Defining a jet width b based on the radial distance where $\bar{U} = 0.5\ U_{\mathrm{m}}$ yields $b/x = 0.130$ and 0.087 for the two experiments, calculated based on the C_u-values. No significant difference could be detected in the counter-flow experiments between the normalized $\bar{U}$-profiles obtained for $N = 1200$ and 1800 rpm.

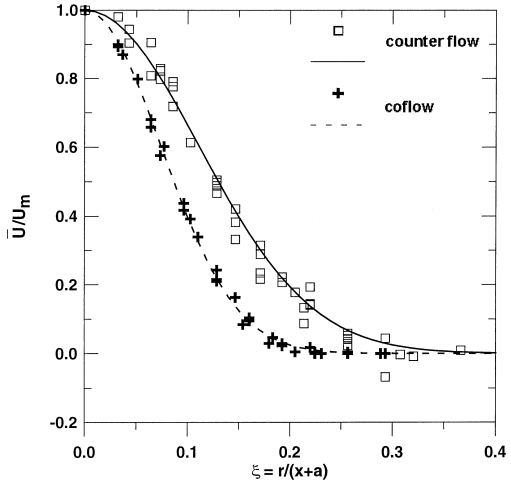

Fig. 6. Normalized mean axial velocity profiles for co-flow and counter-flow in ZEF.

Fig. 7 compares the two Gaussian curves obtained in the present experiments with previous studies on swirling jets. An axisymmetric swirling jet is often characterized by the non-dimensional swirl number S (Chigier and Chervinsky, 1967) defined as

$$S = \frac{G_\phi}{G_x R}, \tag{2}$$

where G_ϕ and G_x, respectively, are given by:

$$G_\phi = 2\pi\rho \int_0^\infty r^2 \overline{UW}\, \mathrm{d}r, \tag{3}$$

$$G_x = 2\pi\rho \int_0^\infty r \left(\overline{U}^2 - \frac{\overline{W}^2}{2} \right) \mathrm{d}r \tag{4}$$

in which ρ is the fluid density. The quantities G_ϕ and G_x may be related to the conservation of axial flux of angular and linear momentum, respectively, and are obtained by integrating the equations of motion for a turbulent, axisymmetric, incompressible, stationary jet (Chigier and Chervinsky, 1967; Pratte and Keffer, 1972). Eq. (3) results from an integration of the equation of motion across the jet for the tangential component, whereas Eq. (4) originates from the integrated axial equation of motion where the pressure term is eliminated by using the radial momentum equation and the turbulence terms are assumed to cancel out.

The swirl number is usually given at the device (the impeller in the present case) and R is taken as the radius of the device itself. The degree of swirl is said to be weak if $S < 0.4$, strong if $S > 0.6$, and moderate in between these values. In the present experiments S was evaluated at $2D$ (where axisymmetry prevailed) to be 0.23 and 0.26 for $N = 1200$ and 1800 rpm, respectively. The counter-flow experiment agrees fairly well with previous studies for similar swirl numbers S, whereas the

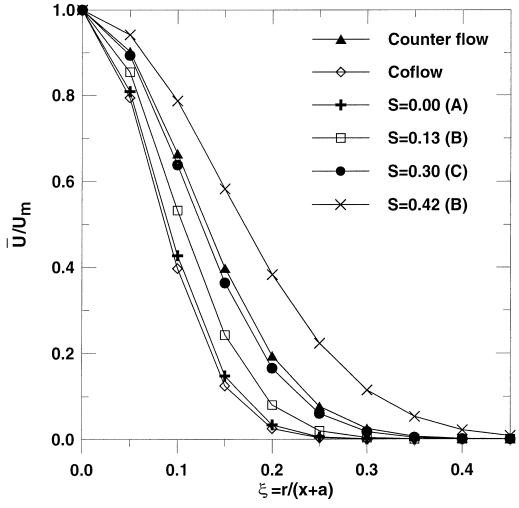

Fig. 7. Comparison between normalized mean axial velocity profiles in the present investigation and other studies on swirling jets (A: Hussein et al. 1994; B: Chigier and Chervinsky 1967; C: Pratte and Keffer 1972).

co-flow experiment produced a jet that is quite similar to a non-swirling jet ($S = 0$) (see Fig. 7). Chigier and Chervinsky (1967) found $C_u = 63$ and 24 for $S = 0.13$ and 0.42, respectively (their experiment for $S = 0.23$ gave $C_u = 27$, which somewhat deviates from the overall trend of the experiments and is not plotted here), and Pratte and Keffer (1972) obtained $C_u = 45$ for $S = 0.30$. Thus, in this respect the jet in the counter-flow is more similar to a free jet, as measured in other experiments, than the jet in the co-flow.

The self-similarity of the other mean velocities was also investigated using W_m to normalize $\bar{W}$, whereas U_m was used for $\bar{V}$ (same as for $\bar{U}$). For the counter-flow experiment the scatter was pronounced, especially at the most downstream measurement locations (Petersson, 1996). However, with a co-flow the jet path was stabilized and the scatter somewhat reduced. Fig. 8(a) and (b) illustrate the normalized $\bar{W}$- and $\bar{V}$-profiles, respectively, as a function of ξ for the co-flow experiment. An empirical equation was fitted to the $\bar{W}$-profiles that produced a single maximum, where $\bar{W} = W_m$, and that decayed towards zero for large ξ-values, as observed in the data:

$$\frac{\overline{W}}{W_m} = \sqrt{2eC_w}\xi e^{-C_w\xi^2}, \tag{5}$$

where C_w is an empirical coefficient. The coefficient C_w was determined to 32 and 56 for the counter-flow and co-flow, respectively, bearing in mind that the counter-flow experiment showed more scatter than the co-flow experiment. Thus, the width of the normalized $\bar{W}$-profiles was substantially smaller for the co-flow compared to the counter-flow, again reflecting the less spread of the jet that occurred in the former experiment (compare with the $\bar{U}$-profiles). Some simple analytical modeling of turbulent swirling jets rely on the existence of self-similar velocity profiles both for $\bar{U}$ and $\bar{W}$ (Chigier and Chervinsky, 1967; Pratte and Keffer, 1972; Larson et al., 1999). The Gaussian shape for $\bar{U}$ has been confirmed by extensive laboratory measurements (also in this study; see Fig. 6), whereas expressions for $\bar{W}$ vary between studies and no general agreement on shape exists. Chigier and Chervinsky (1967) employed a third-order polynomial, although such an expression has the disadvantage that $\bar{W}/W_m$ does not go to 0 as ξ goes to infinity. In this study, the form of Eq. (5) was empirically chosen to fit the necessary physical constraints and the overall fit was judged acceptable for modeling purposes (Larson et al., 1999), although the scatter was significant.

Integrating the continuity equation written in cylindrical coordinates across the jet and assuming a Gaussian profile for $\bar{U}$ yields an equation for how $\bar{V}$ varies with ξ

$$\frac{\overline{V}}{U_m} = \xi e^{-C_u\xi^2} + \frac{e^{-C_u\xi^2} - 1}{2C_u\xi}. \tag{6}$$

Eq. (6) is also plotted in Fig. 8(b), and as can be seen from the figure the fit to the data provided by the equation is only partly successful. The position of zero velocity and the positive and negative velocity peaks are well described, but the magnitude of the positive peak is not well predicted. Also, the measured $\bar{V}$-profiles are typically tailing off at a higher rate in the outer part of the jet compared to Eq. (6). However, the scatter in the plotted data is large and it is not clear that the data support self-similarity for the $\bar{V}$-component over the distance of observation.

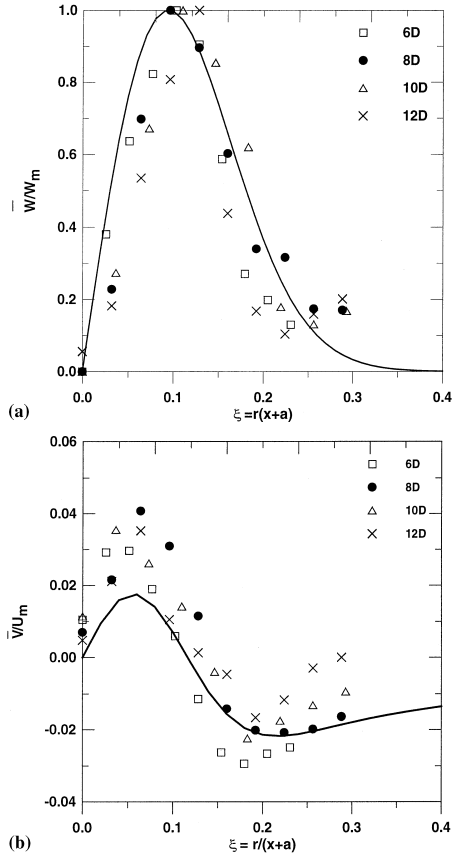

Fig. 8. Normalized mean velocity profiles for co-flow in ZEF, (a) tangential and (b) radial velocities.

3.4. Integral flow development

3.4.1. Spreading angle of jet

The jet tended to spread linearly both in the co-flow and counter-flow, as shown in Fig. 9, where b/D is displayed as a function of x/D for the two experiments. The spreading angle, defined based on b, was 5.0° for the co-flow and 7.4° for the counter-flow. A virtual origin for the jet was possible to define by extrapolating the line describing the jet spread back to $b/D = 0$ giving a virtual source location a distance a upstream the impeller. Such a source has zero mass flux at the origin but angular and linear momentum that produce a swirling jet in the ZEF identical to what the impeller does. The location of the virtual origin was determined to $a = 2D$ and $4D$ for the

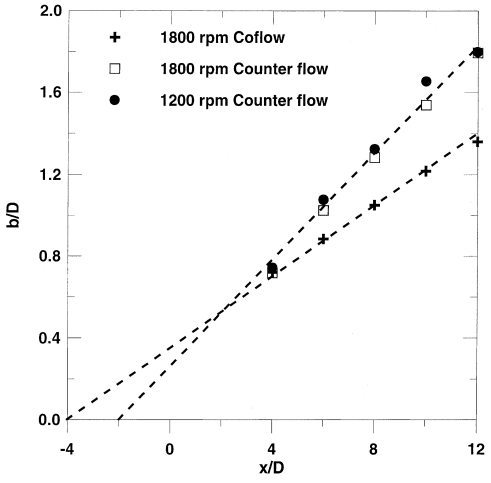

Fig. 9. Radial spread of the jet for co-flow and counter-flow.

counter-flow and co-flow, respectively, reflecting the different spreading angles for the two experiments. These values are similar to the $2.3D$ found by Chigier and Chervinsky (1967) and the $3D$ found by Pratte and Keffer (1972).

The jet was observed to spread at nearly the same angle for the two impeller speeds investigated in the counter-flow experiment. Close to the impeller, a minor increase in the spread of the jet was observed with an increase in the impeller speed. The spread is similar to what Pratte and Keffer (1972) presented for a weakly swirling jet, which was almost twice that of a corresponding non-swirling jet in their experiment. Chigier and Chervinsky (1967) investigated the dependence of the radial spread on the swirl number. They found that the spreading angle increased with S up to about 10° after which the angle was approximately constant. However, it is apparent from previous studies that the spreading angle significantly depends upon the conditions at the discharge point (Chigier and Chervinsky, 1967; Farokhi et al., 1989).

3.4.2. Volume flux and entrainment

The volume flux Q was determined at downstream cross-sections by integrating the measured $\bar{U}$-profiles and the result is displayed in Fig. 10. Various definitions of the jet edge were applied when computing Q, but the difference in results was minor since the jet velocity dropped to negligible values (with respect to the ambient flow velocity) at the measurement points farthest away from the jet centerline. The computed Q-values were normalized with U_pR^2 to allow for comparison between different N (this normalizing quantity will emerge in a dimensional analysis for an impeller). A linear growth in Q with distance downstream occurred that was quite similar for the counter-flow and co-flow experiments, although the most downstream cross-sections in the counter-flow experiment seemed to be affected by the side walls of the flume. Also, U_pR^2 normalized the flow quite well since the volume growth is alike for the different N. In spite of the different spreading angles during the two experiments, the growth in Q with distance downstream was about the same.

The rate of entrainment can be determined based on the calculated volume flux. The amount of fluid entrained up to a given location is $Q - Q_0$, where Q_0 is the flow at the impeller, and an entrainment coefficient, (K_e) may be defined as (compare Chigier and Chervinsky, 1967)

$$K_e = \frac{D}{Q_0}\frac{dQ}{dx}. \tag{7}$$

The increase in volume flux is almost constant up to approximately $10D$ and K_e was determined from a fitted line between sections $1D$–$10D$. For both co-flow and counter-flow ($N = 1200$ and 1800 rpm), the entrainment coefficient was determined to be approximately 0.4. This value is lower than that obtained by Chigier and Chervinsky (1967), who calculated $K_e = 0.5$ for a jet with a similar degree of swirl. However, $K_e = 0.4$ agrees well with the results of Rose (1962) (also similar degree of swirl). For a free non-swirling jet Chigier and Chervinsky (1967) determined K_e to be 0.32 in agreement with Albertson et al. (1950) and Ricou and Spalding (1960). Thus, an impeller jet has an entrainment rate that is higher than a non-swirling jet.

The computed K_e- value for the impeller jet was based on the volume flux in both the ZFE and ZEF. The value $K_e = 0.32$ obtained for non-swirling jets is only valid for the ZEF, and the entrainment rate is much lower in the ZFE. Albertson et al. (1950) used a second-degree polynomial to describe Q/Q_0 in the ZFE for a non-swirling jet, where the ZFE extended to $x/D = 6.2$. An average value on K_e may be calculated for the ZFE from Albertson et al. (1950) to 0.16. Thus, the impeller-generated jet entrains more water in both the ZFE and ZEF, but the difference is much more marked in the ZFE.

3.4.3. Momentum flux

The swirl number S is derived from the ratio between G_ϕ and G_x (Eq. (2)), which in turn arises from the equations of motions in the tangential and axial direction, respectively. The quantity G_ϕ may be interpreted as the axial flux of angular momentum, whereas G_x represents the axial flux of linear momentum corrected for the pressure. Thus, for a swirling jet unaffected by an ambient flow S should be a constant that is independent of the downstream location. However, in the present experiments a flow occurred in the ambient and G_x will experience an increase in the downstream direction for the co-flow, whereas a counter-flow should act as a momentum sink for the jet. The G_x-values calculated from the data clearly showed the decrease in G_x for the counter-flow case, as illustrated in Fig. 11 (G_x was normalized with $\rho U_p^2R^2$ to allow for comparison between different N), although the decrease was too large to be explained purely by the counter-flow. This difference was attributed to the turbulent fluctuations (Petersson et al., 1996a), although pressure and wall shear effects may have influenced G_x. However, detailed measurements of the water surface elevation along the flume did not reveal any differences in elevation. In the co-flow experiment the

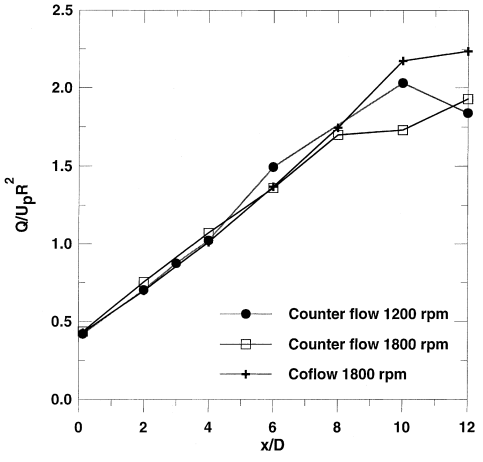

Fig. 10. Normalized volume flux as a function of distance downstream for co-flow and counter-flow.

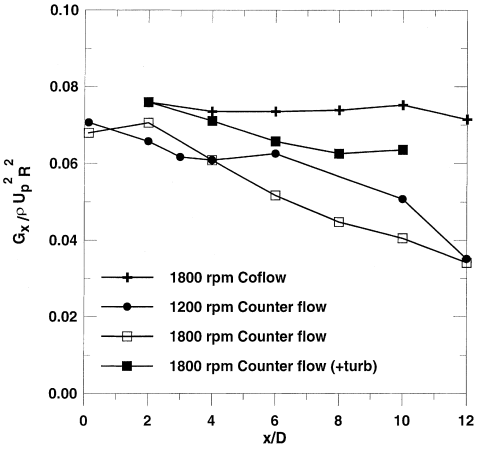

Fig. 11. Normalized momentum flux as a function of distance downstream for co-flow and counter-flow.

employed ambient velocity was not large enough to significantly change G_x over the distance of observation. The computed axial flux of angular momentum G_ϕ did not vary much at the different downstream locations, both in the case of co-flow and counter-flow.

Eq. (4) is typically employed as a first approximation to evaluate G_x, which is often referred to as the jet thrust since it contains a pressure contribution (Pratte and Keffer, 1972; Hussein et al., 1994). It is a first approximation because Eq. (4) is based on the assumption that the turbulent fluctuations are of the same order and cancel out in the derivation (Chigier and Chervinsky, 1967). However, analysis of the measurements from the counter-flow experiment showed that the root-mean-square (rms) value of the axial velocity component (u) is consistently larger than the rms value for the radial (v) and tangential (w) component. Thus, an estimate of G_x is needed that includes the normal stresses (Pratte and Keffer, 1972).

$$G_x = 2\pi\rho \int_0^\infty r \left(\overline{U}^2 - \frac{\overline{W}^2}{2} + u^2 - \frac{w^2 + v^2}{2} \right) \mathrm{d}r \tag{8}$$

Fig. 11 also illustrates the momentum flux evaluated by using Eq. (8) for $N = 1800$ rpm (complete measurements were not obtained at all locations of the normal stresses to allow evaluation of Eq. (8) for $N = 1200$ rpm); the decrease in G_x that still occurred downstream of the impeller using this equation is fully explainable in terms of the return flow. In the co-flow experiment the rms values were similar in magnitude (Peterson, 1996), which fulfills the basic assumption behind Eq. (4) making this expression sufficient for computing G_x. The main reason why the rms values differ in the counter-flow experiment was the long-periodic oscillations previously mentioned that significantly affected u far away from the impeller.

4. Conclusions

The laboratory measurements carried out in this investigation displayed the effects of a weakly flowing ambient fluid on the development of a swirling jet generated by an impeller. Two main cases were explored, namely the jet evolution in a closed-off flume and in an open flume with a base flow. The former experimental setup involved a return flow (counter-flow) from which the water entrained in the jet originated, whereas in the open-flume case the entrained water came from the base flow (co-flow). Measurements of all three velocity components (axial, tangential, and radial) were performed with an LDV at selected downstream cross sections. The focus of this paper was on the mean velocities and the integral flow development, although the velocity unsteadiness was measured as well in the experiments.

The principal features of the spatial development of the mean jet velocity components were similar for the counter-flow and the co-flow, although the numerical values of basic jet properties differed some distance downstream of the impeller. In the vicinity of the impeller ($x < 2D$) there was little difference in the measured mean velocity profiles, and in this region the profiles were mainly a function of the impeller characteristics (e.g., diameter, rotational speed, number of blades, and blade shape). Further downstream the ambient flow conditions had a pronounced effect on the measured mean velocity profiles, where the counter-flow produced an increased jet width implying a larger spreading angle. The jet tended to spread linearly both in the counter-flow and co-flow case at an angle of 7.4° and 5.0°, respectively.

The periodicity induced by the impeller in the mean velocities was found to completely disappear after approximately $2D$, and already at $1D$ the effects were quite small. In this investigation, the border between the zone of flow establishment and the zone of established flow was made based on self-similarity in the mean axial velocity profile. At about $4D$ a Gaussian curve described the mean axial velocity well, both for the counter-flow and co-flow. However, the coefficient in the Gaussian curve had markedly different values for the counter-flow and co-flow, reflecting the different jet spread in the two cases. The mean tangential velocity also indicated self-similarity at this location, even though the scatter was marked, whereas the radial component displayed too much scatter to confirm any self-similarity.

The volume flux increased linearly with distance downstream, and the counter-flow and co-flow displayed a similar growth rate. Thus, even though the spreading angles were different for the two cases the volume growth was almost identical. It is hypothesized that the generated jets are quite similar in the two cases, even further downstream than $2D$, but the counter-flow causes a slow lateral oscillation of the jet that viewed on a longer time scale (over which measurements were made) makes the jet look wider. In contrast, a small base flow stabilizes the jet path so that a narrower jet is observed in the measurements. The slow oscillation was produced through a complicated interaction between the jet and the return flow. This interaction also affected the measured axial rms velocity, making it consistently larger than the tangential and radial rms velocities, especially at larger distances from the impeller. In the estimates of the downstream momentum flux for the counter-flow case, this anisotropy had to be taken into account.

Comparing the results from the present investigation with other studies on free swirling jets (generated by other means) showed that the jet developing in the counter-flow displayed a similar spread to what has previously been observed. The jet in the co-flow had a spread that was close to a non-swirling jet. The volume flux and entrainment rate in the zone of established flow were in agreement with some previous studies, and notably larger than a non-swirling jet. In the zone of flow establishment. the difference in the entrainment rate between the impeller jet and a non-swirling jet was even more pronounced than in the zone of established flow.

Acknowledgements

This research was supported by the Swedish Research Council for Engineering Sciences (TFR Dnr 93-80). The authors wish to thank Magnus Fahlgren at ITT Flygt AB for supplying the experimental impeller setup used in the investigation. ML likes to acknowledge the financial support from the Sasakawa Foundation for a research visit to the University of Tokyo. The help received from the people at the Coastal Engineering Laboratory of the University of Tokyo during ML's visit is greatly appreciated. Two anonymous reviewers provided highly constructive and stimulating criticism of the paper and considerably improved it.

References

Abramovich, G.N., 1963. The Theory of Turbulent Jets. Massachusetts Institute of Technology, MIT Press, Cambridge, MA.

Albertson, M.L., Dai, Y.B., Jensen, R.A., Rouse, H., 1950. Diffusion of submerged jets. Transactions of the American Society of Civil Engineers 115 Paper No. 2409, 639–697.

Biggers, J.C., Orloff, K.L., 1975. Laser velocimeter measurements of the helicopter rotor-induced flow field. Journal of the American Helicopter Society 20, 2–10.

Chigier, N.A., Chervinsky, A., 1967. Experimental investigations of swirling vortex motion in jets. Journal of Applied Mechanics 34, 443–451.

Fahlgren, M., Tammelin, J., 1992. The 3-D velocity field near a submerged hydrofoil impeller. Scientific Impeller, ITT Flygt AB, 1 (1) 49–57.

Farokhi, S., Taghavi, R., Rice, E.J., 1989. Effect of initial swirl distribution on the evolution of a turbulent jet. AIAA Journal 27 (6), 700–706.

Hamill, G.A., Johnston, H.T., 1993. The decay of maximum velocity within the initial stages of a propeller wash. Journal of Hydraulic Research 31 (5), 605–613.

Hussein, J.H., Capp, S.P., George, W.K., 1994. Velocity measurements in a high-Reynolds-number momentum-conserving axisymmetric turbulent jet. Journal of Fluid Mechanics 258, 31–75.

Hyun, B-S., Patel, V.C., 1991a. Measurements in the flow around a marine propeller at the stern of an axisymmetric body. Part 1: Circumferentially averaged flow. Experiments in Fluids 11, 33–44.

Hyun, B.-S., Patel, V.C., 1991b. Measurements in the flow around a marine propeller at the stern of an axisymmetric body. Phase 2: averaged flow. Experiments in Fluids 11, 105–117.

Jönsson, L., Rissler, S., 1991. The use of mixers for improving water quality in reservoirs, lakes, and harbors. In: Proceedings of the European Conference on Advances in Water Resources Technology. A.A. Balkema, Rotterdam, The Netherlands, pp. 407–416.

Kobayashi, S., 1981. Experimental methods for the prediction of the effect of viscosity on propeller performance. Ph.D. Thesis, Department of Ocean Engineering, Massachusetts Institute of Technology, MA.

Larson, M., Petersson, P., Jönsson, L., 1999. Analytical model of an impeller-generated turbulent jet in a weak co-flow and counter-flow. Journal of Fluids Engineering (submitted).

Lepicovsky, J., 1988. Laser velocimeter measurements in a model propeller flowfield. Journal of Fluids Engineering 110, 350–354.

Lepicovsky, J., Bell, W.A., 1984. Aerodynamic measurements about a rotating propeller with a laser velocimeter. Journal of Aircraft 21 (4), 264–271.

Min, K.-S., 1978. Numerical and experimental methods for the prediction of field point velocities around propeller blades. Ph.D. Thesis, Department of Ocean Engineering, Massachusetts Institute of Technology, MA.

Petersson, P., 1996. Laser doppler velocity measurements in an impeller-generated turbulent jet. Report 3195, Department of Water Resources Engineering, Lund University, Lund.

Petersson, P., Larson, M., Jönsson, L., 1996a. Measurements of the velocity field downstream an impeller. Journal of Fluids Engineering 118 (3), 602–610.

Petersson, P., Larson, M., Jönsson, L., 1996b. Impeller-generated jets in weak co-flow and counter-flow. In: Proceedings of the Second International Conference on Hydrodynamics, vol. I. Hong Kong, pp. 583–588.

Pratte, B.D., Keefer, J.F., 1972. The swirling turbulent jet. Journal of Basic Engineering 93, 739–748.

Ricou, F.P., Spalding, D.B., 1960. Measurements of entrainment by axisymmetrical turbulent jets. Journal of Fluid Mechanics 11, 21–32.

Rose, W.G., 1962. A swirling round turbulent jet. Journal of Applied Mechanics 29, 615–625.

Shih, C., Ho, C.-M., 1994. Three-dimensional recirculation flow in a backward facing step. Journal of Fluids Engineering 116, 228–232.

Stephens, R., Imberger, J., 1993. Reservoir destratification via mechanical mixers. Journal of Hydraulic Engineering 119 (4), 438–457.

Strazisar, A.J., Powell, J.A., 1981. Laser anemometer measurements in a transonic axial flow compressor rotor. Journal of Engineering for Power 103, 430–437.

Townsend, A.A., 1976. The Structure of Turbulent Shear Flow. Cambridge University Press, Cambridge, MA.